Fusion Engineering and Design 86 (2011) 1107–1111

Contents lists available at ScienceDirect

Fusion Engineering and Design

journal homepage: www.elsevier.com/locate/fusengdes

Multivariable model-based shape control for the National Spherical Torus Experiment (NSTX)

W. Shi[a,*], M. Alsarheed[a], E. Schuster[a], M.L. Walker[b], J. Leuer[b], D.A. Humphreys[b], D.A. Gates[c]

[a] Department of Mechanical Engineering and Mechanics, Lehigh University, Bethlehem, PA 18015, USA
[b] General Atomics, San Diego, CA 92121, USA
[c] Princeton Plasma Physics Laboratory, Princeton, NJ 08543, USA

ARTICLE INFO

Article history:
Available online 16 April 2011

Keywords:
NSTX
Shape control
Robust control
Singular value decomposition

ABSTRACT

Plasma current, position and shape control is a challenging problem due to the strong coupling between the different parameters describing the shape of the plasma. By leveraging the availability of rtEFIT, this paper proposes a robust model-based multi-input–multi-output (MIMO) controller to provide real-time shaping, position stabilization and current regulation in NSTX. The proposed controller is composed of three loops: the first loop is devoted to plasma current regulation, the second loop is dedicated to plasma radial and vertical position stabilization, and the third loop is used to control the plasma shape. This control approach transforms the shape control problem into an output tracking problem. The goal is the minimization of a quadratic cost function that describes the tracking error in steady state. A singular value decomposition (SVD) of the nominal plasma model is carried out to decouple and identify the most relevant control channels. The H_∞ technique is used to minimize the tracking errors and optimize input efforts. Computer simulation results illustrate the performance of the robust model-based shape controller, showing potential for improving the performance of present non-model-based controllers.

1. Introduction

The plasma shape requirements in a practical, highly efficient tokamak are very stringent. The extreme shapes that must be achieved, intrinsic instability in the plasma vertical position (the more shaped the plasma, the more unstable), large number of control inputs (coil voltages) and control outputs (geometrical parameters and plasma current), and demanding regulation requirements make this problem very challenging [1].

NSTX presents a unique control challenge relative to other tokamaks, in that there are no coils on the inboard side of the plasma and just a small number of coils on the outboard side. The strong coupling between the different geometrical parameters describing the shape of the plasma calls for a model-based, multivariable approach to obtain improvements in closed-loop performance. The recent implementation of the real-time equilibrium reconstruction code rtEFIT [2] in NSTX allows plasma shaping by controlling the magnetic flux at the plasma boundary. A non-model-based, empirically tuned, single-input–single-output (SISO), proportional-integral-derivative (PID) shape controller that exploits this capability has been recently proposed [3]. Alternatively, we present a robust model-based multi-input–multi-output (MIMO) controller to provide real-time shaping, position stabilization and current control in the presence of disturbances and uncertainties. Singular value decomposition (SVD) is used for decoupling and identification of the most relevant control channels [4]. The control design is based on linear plasma response models derived from fundamental physics assumptions.

2. NSTX model description and control approach

The system composed of plasma, shaping coils, and passive structure can be described using circuit equations derived from Faraday's Law, and radial and vertical force balance relations for a particular plasma equilibrium. In addition, rigid radial and vertical displacement of the equilibrium current distribution is assumed, and a resistive plasma circuit equation is specified [5]. The result is a circuit equation describing the linearized response, around a particular plasma equilibrium, of the conductor-plasma system to voltages applied to active conductors. For control design and simulation purposes, the linearized plasma response model can be written in state space form

$$\dot{x} = Ax + Bu, \quad \delta y = C\delta x \tag{1}$$

where $x = [I_c^T I_v^T I_p^T]^T$ and $u = [V_c^T 0 V_{no}^T]^T$, with I_c, I_v, and I_p representing currents in PF coils, vessel, and plasma, respectively, V_c

* Corresponding author. Tel.: +1 610 758 3707.
E-mail address: wenyu.shi@lehigh.edu (W. Shi).

0920-3796/$ – see front matter © 2011 Elsevier B.V. All rights reserved.
doi:10.1016/j.fusengdes.2011.03.023

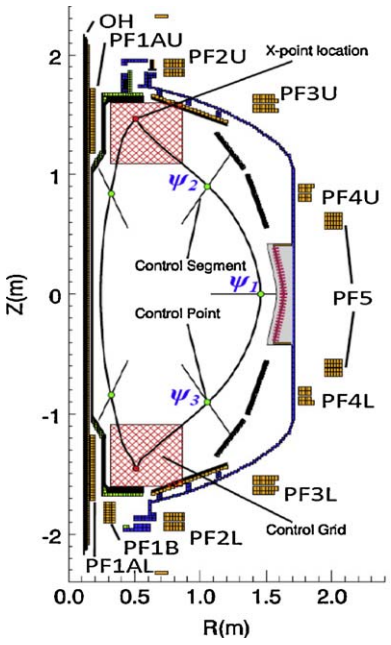

Fig. 1. NSTX isoflux control configuration.

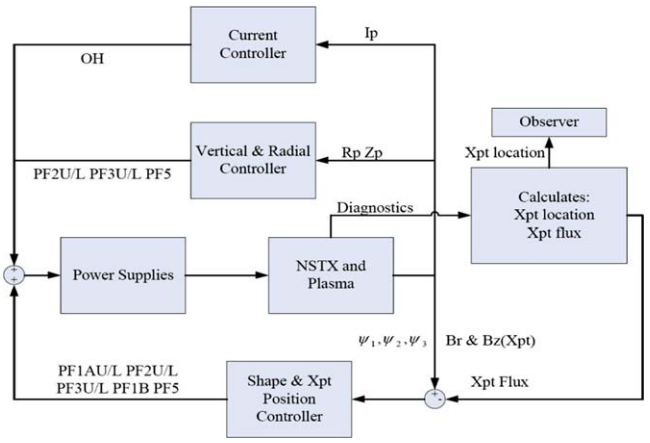

Fig. 2. NSTX control system architecture.

representing the vector of voltages applied to the PF coils, and V_{no} representing the effective voltage applied to drive plasma current by noninductive sources (no noninductive current source is considered in this work, i.e., $V_{no} = 0$). We define $\delta T = T - T_{eq}$, for $T \in \{x, y\}$, where the subscript "*eq*" denotes values at the equilibrium from which the model is derived.

Isoflux control exploits the capability of the real time EFIT plasma shape reconstruction algorithm to calculate magnetic flux at specified locations within the tokamak vacuum vessel. Fig. 1 shows a typical isoflux control configuration in NSTX. Real time EFIT can calculate very accurately the value of flux in the vicinity of the plasma boundary. Thus, the controlled parameters are the values of flux at prespecified control points along with the X-point *r* and *z* positions. By requiring that the flux at each control point be equal to the same constant value, the control forces the same flux contour to pass through all of these control points. By choosing this constant value equal to the flux at the X-point, this flux contour must be the last closed flux surface or separatrix.

3. Control system design

The proposed control architecture shown in Fig. 2 is composed of three loops. The first loop is devoted to plasma current regulation (PID controller), the second loop is dedicated to plasma radial and vertical position stabilization (PID controller), and the third loop is used to control the plasma shape and X-point location (multi-input–multi-output robust controller).

The ohmic (OH) coil is dedicated to plasma current regulation. The proposed plasma current controller is written as

$$V_{OH} = G_P^{I_p} \Delta I_p + G_I^{I_p} \int_0^t \Delta I_p dt + G_D^{I_p} \frac{d\Delta I_p}{dt}, \tag{2}$$

where $\Delta I_p = I_p - I_P^{ref}$ with I_P^{ref} denoting the reference plasma current. The parameters $G_P^{I_p}$, $G_I^{I_p}$, and $G_D^{I_p}$ are the plasma current PID gains.

Poloidal field coils PF2U/L, PF3U/L, and PF5 are used for plasma radial position control while poloidal field coils PF2U/L and PF3U/L are used for plasma vertical position control. The selection of these sets of actuators is the result of a sensitivity study carried out for the steady-state transfer function. The contribution to the coil voltages by the proposed radial position controller is written as $\Delta V_{PF2_R}^{U/L} = \Delta V_{PF3_R}^{U/L} = \Delta V_{PF5_R} = V_{R_p}$, with

$$V_{R_p} = G_P^{R_p} \Delta R_P + G_I^{R_p} \int_0^t \Delta R_P dt + G_D^{R_p} \frac{d\Delta R_P}{dt} \tag{3}$$

where $\Delta R_p = R_p - R_P^{ref}$ with R_P^{ref} denoting the reference plasma radial position. The parameters $G_P^{R_p}$, $G_I^{R_p}$, and $G_D^{R_p}$ are the plasma radial position PID gains. The contribution to the coil voltages by the proposed vertical position controller is written as $\Delta V_{PF2_Z}^{j} = \Delta V_{PF3_Z}^{j} = V_{Z_p}(j)$, with

$$V_{Z_p}(j) = (-1)^j \left(G_P^{Z_p} \Delta Z_P + G_I^{Z_p} \int_0^t \Delta Z_P + G_D^{Z_p} \frac{d\Delta Z_P}{dt} \right) \tag{4}$$

where the superscript $j \in \{0, 1\}$ refers to upper and lower PF coils respectively. The parameters $G_P^{Z_p}$, $G_I^{Z_p}$, and $G_D^{Z_p}$ are the plasma vertical position PID gains. The voltage offset ΔV_{PFi}^{j} is then added to the voltage shape control requests.

The separate design of the plasma current and position controllers transforms the shape control problem into an output tracking problem. The tracking error is defined as $e(t) = r(t) - y(t)$, with the system output $y(t)$ defined as the magnetic fluxes at three control points and the magnetic field components at the desired X-point location, i.e., $y = \begin{bmatrix} \psi_1 & \psi_2 & \psi_3 & B_r & B_z \end{bmatrix}^T$. The contribution to the coil voltages by the shape controller is written as

$$\left[\Delta V_{PF1A_S}^{U/L} \Delta V_{PF1B_S} \Delta V_{PF2_S}^{U/L} \Delta V_{PF3_S}^{U/L} \Delta V_{PF5_S} \right]^T = \hat{K} e.$$

The plasma shape and X-point location control algorithm can be summarized by the following steps: (1) calculate ψ_1, ψ_2 and ψ_3 at the control points, and B_r and B_z at the desired X-point location; (2) estimate the actual X-point location, compute the flux at this point and define this value as ψ_{ref}; (3) make the flux at the control points track the flux ψ_{ref} at the X point and make B_r and B_z at the desired X-point location go to zero. There are no reference points in the upper and inboard sections to avoid clash with the radial and vertical position controllers.

The relation between inputs and outputs in the linear model (1) can be expressed in terms of its transfer function $P(s) = Y(s)/U(s) = (C(sI - A)^{-1}B + D)$, where s denotes the Laplace variable and $Y(s)$ and $U(s)$ denote the Laplace transform of output and input vectors respectively. Assuming constant references $\bar{r}$ and closed-loop stabilization, the system will reach steady state as $t \to \infty$. It is possible then to define $\bar{y} = \lim_{t\to\infty} y(t)$, $\bar{u} = \lim_{t\to\infty} u(t)$,

$\bar{e} = \lim_{t\to\infty} e(t) = \bar{r} - \bar{y}$. By invoking the final value theorem, we can express the closed-loop system in steady state as

$$\bar{y} = \bar{P}\bar{u} = -CA^{-1}B\bar{u}, \quad \bar{u} = \bar{\hat{K}}\bar{e} = \bar{\hat{K}}(\bar{r} - \bar{y}), \tag{5}$$

where $\hat{K}(s)$ is the controller transfer function ($\bar{\hat{K}} = \hat{K}(0)$).

We consider the problem of minimizing a steady-state cost function given by

$$\bar{J} = \lim_{t\to\infty} e^T(t)Qe(t) = \bar{e}^T Q\bar{e} \tag{6}$$

where $Q \in \Re^{p\times p}$ (P is the number of outputs) is a positive definite weighting matrix for the tracking error. In order to weight the control effort, another positive definite weighting matrix $R \in \Re^{m\times m}$ (m is the number of inputs) is also introduced. The choice of the weighting matrices Q and R is usually the outcome of an iterative design process in which the objective is to minimize the tracking error while keeping the control actuation within physical limits.

We define the "weighted" steady-state transfer function, and its singular value decomposition, as

$$\tilde{P} = Q^{1/2}\bar{P}R^{-1/2} = USV^T \tag{7}$$

where $S = diag(\sigma_1, \sigma_2, \cdots, \sigma_m) \in \Re^{m\times m}$, $U \in \Re^{p\times m}$ ($U^TU = I$), and $V \in \Re^{m\times m}$ ($V^TV = VV^T = I$). Note that the steady-state input–output relation can now be expressed as

$$\bar{y} = \bar{P}\bar{u} = Q^{-1/2}\tilde{P}R^{1/2}\tilde{u} = Q^{-1/2}USV^TR^{1/2}\tilde{u}. \tag{8}$$

By invoking SVD properties, we can note that the columns of the matrix $Q^{-1/2}US$ define a basis for the subspace of obtainable steady-state output values and we can always write

$$\bar{y} = Q^{-1/2}US\bar{y}^* \Leftrightarrow \bar{y}^* = S^{-1}U^TQ^{1/2}\bar{y} \tag{9}$$

with $\bar{y}^* \in \Re^m$. We will only be able to track in steady-state the component of the reference vector $\bar{r}$ that lies in this subspace. We write then the reference vector as the sum of a trackable component $\bar{r}_t$ and a non-trackable component $\bar{r}_{nt}$, i.e., $\bar{r} = \bar{r}_t + \bar{r}_{nt}$, where

$$\bar{r}_t = Q^{-1/2}US\bar{r}^* \Leftrightarrow \bar{r}^* = S^{-1}U^TQ^{1/2}\bar{r} \tag{10}$$

with $\bar{r}^* \in \Re^m$ and $S^{-1}U^TQ^{1/2}\bar{r}_{nt} = 0$.

Note that by defining $\bar{u}^* = V^TR^{1/2}\tilde{u}$, the relationship between $\bar{y}^*$ and $\bar{u}^*$ is obtained by using (8) as

$$\bar{y}^* = S^{-1}U^TQ^{1/2}\bar{y} = S^{-1}U^TQ^{1/2}Q^{-1/2}USV^TR^{1/2}\tilde{u} = \bar{u}^* \tag{11}$$

and one-to-one relationships between inputs and outputs are obtained. The new system is a square decoupled system.

The steady state error can now be rewritten as

$$\bar{e} = \bar{r} - \bar{y} = Q^{-1/2}US(\bar{r}^* - \bar{y}^*). \tag{12}$$

Substituting this expression in (6), the performance index is now expressed as

$$\bar{J} = (\bar{r}^* - \bar{y}^*)^TS^2(\bar{r}^* - \bar{y}^*) = \sum_{i=1}^{m}\sigma_i^2(\bar{r}_i^* - \bar{y}_i^*)^2. \tag{13}$$

The purpose of the shape control is to minimize the performance index $\bar{J}$. However, it is usually the case where $\sigma_1 > \cdots \sigma_k \gg \sigma_{k+1} > \cdots > \sigma_m > 0$. Note that the singular value σ_i, for $i = 1, \ldots, m$, is the weight parameter for the ith component of the tracking error. Therefore, it is possible that in the intent of minimizing $\bar{J}$ in (13) we spend lot of control effort in minimizing ith components of the tracking error, for $i > k$, that have a very small contribution to the overall value of the cost function. To avoid spending lot of control effort for a marginal improvement of the cost function value, the cost function is rewritten as

$$\bar{J}_s = \sum_{i=1}^{k}\sigma_i^2(\bar{r}_i^* - \bar{y}_i^*)^2. \tag{14}$$

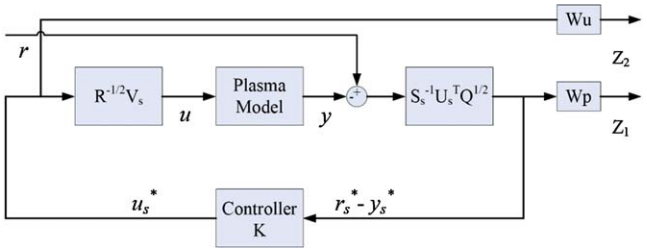

Fig. 3. H_∞ control formulation.

By partitioning the singular value set in significant singular values S_s and negligible singular values S_n, we can write $U = [U_sU_n]$, $V = [V_sV_n]$, $S = diag(S_s, S_n)$, and obtain

$$\bar{J}_s = \sum_{i=1}^{k}\sigma_i^2(\bar{r}_i^* - \bar{y}_i^*)^2 = (\bar{r}_s^* - \bar{y}_s^*)^TS_s^2(\bar{r}_s^* - \bar{y}_s^*) \tag{15}$$

with $\bar{r}_s^* = S_s^{-1}U_s^TQ^{1/2}\bar{r}$, $\bar{y}_s^* = S_s^{-1}U_s^TQ^{1/2}\bar{y}$, $\bar{u}_s^* = V_s^TR^{1/2}\bar{u}$.

Based on the outcome of the SVD, the control architecture shown in Fig. 3 is proposed, where two frequency-dependent weighting functions W_p and W_u are introduced. The mixed sensitivity H_∞ control technique is used to find a $k \times k$ controller that minimizes the tracking error $r_s^* - y_s^*$ as $t \to \infty$, and therefore $\bar{J}_s$ in (15), while minimizing the control effort u_s^*. The signals of the general control configuration are defined as the control input $\tilde{u} = u_s^*$, the tracking error $\tilde{e} = r_s^* - y_s^*$, the exogenous reference $\tilde{r} = \bar{r}$ and the external performance signal $\tilde{z}$.

Using the Laplace Transform we can obtain a frequency-domain representation of the overall system. The plant $G(S)$ is the transfer function from the input signals $\begin{bmatrix}\tilde{r}^T & \tilde{u}^T\end{bmatrix}^T$ to the output signals $\begin{bmatrix}\tilde{z}_1^T & \tilde{z}_2^T & \tilde{e}^T\end{bmatrix}^T$, i.e.,

$$\begin{bmatrix}\tilde{z}\\ \tilde{e}\end{bmatrix} = \begin{bmatrix}\tilde{z}_1\\ \tilde{z}_2\\ \tilde{e}\end{bmatrix} = G(s)\begin{bmatrix}\tilde{r}\\ \tilde{u}\end{bmatrix} = \begin{bmatrix}G_{11}(s) & G_{12}(s)\\ G_{21}(s) & G_{22}(s)\end{bmatrix}\begin{bmatrix}\tilde{r}\\ \tilde{u}\end{bmatrix},$$

where

$$G_{11} = \begin{bmatrix}W_pS_s^{-1}U_s^TQ^{1/2}\\ 0\end{bmatrix} \qquad G_{22} = -S_s^{-1}U_s^TQ^{1/2}PR^{-1/2}V_s$$
$$G_{12} = \begin{bmatrix}-W_pS_s^{-1}U_s^TQ^{1/2}PR^{-1/2}V_s\\ W_u\end{bmatrix} \qquad G_{21} = S_s^{-1}U_s^TQ^{1/2}$$

We define the transfer function M_s as

$$M_s = (I + S_s^{-1}U_s^TQ^{1/2}PR^{-1/2}V_sK)^{-1}S_s^{-1}U_s^TQ^{1/2}, \tag{16}$$

and write the closed-loop transfer function as

$$T_{zr} = F_l(G, K) = G_{11} + G_{12}K(I - G_{22}K)^{-1}G_{21} = \begin{bmatrix}W_pM_s\\ W_uKM_s\end{bmatrix} \tag{17}$$

where $F_l(G, K)$ is the lower linear fractional transform (LFT).

We seek a controller $K(s)$ that stabilizes the system and minimizes the H_∞ norm of the transfer function $T_{zr}(G, K)$, i.e.,

$$\min_{K(s)}||T_{zr}(G, K)_\infty|| = \min_{K(s)}(\sup_\omega \bar{\sigma}[T_{zr}(G, K)(j\omega)]) = \min_{K(s)}\left\|\begin{matrix}W_pM_s\\ W_uKM_s\end{matrix}\right\|_\infty$$

where $\bar{\sigma}$ represents the maximum singular value. This statement defines a mixed sensitivity H_∞ control problem, where the goal is to minimize both the error tracking (W_pM_s) and the control effort

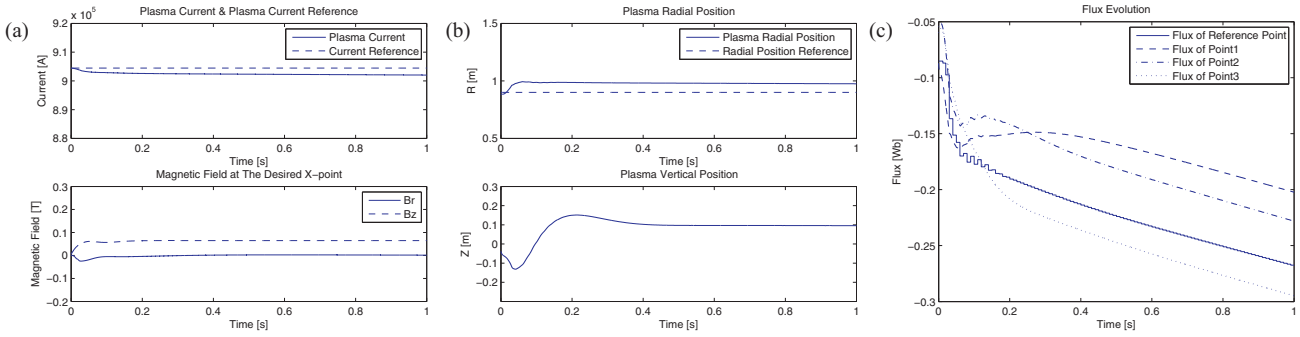

Fig. 4. Closed-loop evolution: (a) plasma current and magnetic field; (b) plasma radial and vertical position; (c) magnetic flux at the control points.

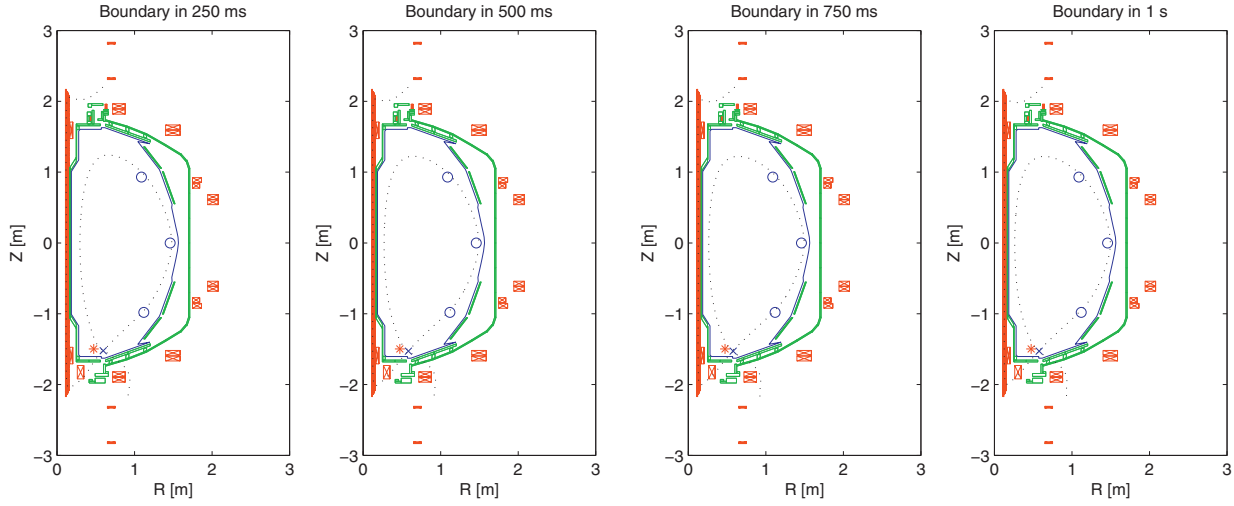

Fig. 5. Plasma boundary at 250 ms, 500 ms, 750 ms and 1 s.

$(W_u K M_s)$ at the same time. The weighting functions W_p and W_u are parameterized as

$$W_p(s) = \frac{\frac{s}{M_1} + w_{b1}}{s + w_{b1}A_1} K_p, \quad W_u(s) = \frac{s + w_{b2}A_2}{\frac{s}{M_2} + w_{b2}} K_u$$

where the coefficients M_i, A_i, w_{bi}, for $i = 1, 2$, as well as K_p and K_u, are design parameters in the H_∞ control synthesis.

The overall plasma shape and X-point location controller can be written as ($E(s)$ denotes the Laplace transform of $e(t)$)

$$\hat{K}(s) = \frac{U(s)}{E(s)} = R^{-1/2} V_s K(s) S_s^{-1} U_s^T Q^{1/2}. \tag{18}$$

4. Simulation results

The reference values in this simulation study for the radial position, vertical position, plasma current and X-point location are those of the equilibrium (#124616) around which the linearized model is obtained. The reference value for the flux at the control points is equal to that of the X-point, which is computed every 10 ms.

The plasma current is controlled by the PID control loop (2). Fig. 4(a) (top) shows the time evolution for the plasma current and compare it with its reference. The tracking error is less than 0.5%. The plasma positions are controlled by the two independent PID control loops (3) and (4). The time responses for the plasma radial and vertical positions are shown in Fig. 4(b). The vertical position is stabilized by the controller and a steady-state value is quickly achieved. Fig. 4(c) shows both the flux at the X-point and the flux at the three control points (ψ_1, ψ_2, and ψ_3). The flux at the control points track the flux at the X-point with a small constant tracking error. After about 400 ms, the system achieves steady-state tracking errors of less than 0.02 Wb. The components of the magnetic field at the desired X-point are shown in the Fig. 4(a) (bottom). The steady-state errors are less than 0.05 T. A series of four plasma boundary shapes at different times during the simulated discharge is shown in Fig. 5. The blue circles represent the control points, the blue x-mark represents the actual location of the X-point and the red asterisk represents the reference location of X-point. The PF coil voltages are regulated according to the H_∞ control law (18).

5. Conclusion

The proposed model-based controller, which was tested in simulations, shows potential for expanding present experimental control capabilities. A more exhaustive and realistic simulation study is part of our future work before experimental validation. Ideally this study should include free-boundary simulations, real-time boundary reconstruction, synthetic noise in the measurements and simulated disturbances.

Acknowledgements

Work supported by the NSF CAREER award program (ECCS-0645086) and the U.S. DOE (DE-FG02-09ER55064).

References

[1] G. Ambrosino, R. Albanese, Magnetic control of plasma current position and shape in Tokamaks, IEEE Control Systems Magazine 25 (5) (2005) 76–92.

[2] J.R. Ferron, M.L. Walker, L.L. Lao, H.E. St. John, D.A. Humphreys, J.A. Leuer, Real time equilibrium reconstruction for tokamak discharge control, Nuclear Fusion 38 (1998) 1055–1066.
[3] D.A. Gates, J.R. Ferron, M. Bell, T. Gibney, R. Johnson, R.J. Marsala, et al., Plasma shape control on the National Spherical Torus Experiment (NSTX) using real-time equilibrium reconstruction, Nuclear Fusion 46 (2006) 17–23.
[4] G. Ambrosino, M. Ariola, A. Pironti, F. Sartori, Design and implementation of an output regulation controller for the JET tokamak, IEEE Transactions on Control Systems Technology 16 (6) (2008) 1101–1111.
[5] M. Walker, D. Humphreys, Valid coordinate systems for linearized plasma shape response models in tokamaks, Fusion Science and Technology 50 (4) (2006) 473–489.